


Cite this: *Dalton Trans.*, 2023, **52**, 13769

Formation of MnO₂-coated ITO electrodes with high catalytic activity for enzymatic glucose detection†

Veronika Poltavets,^{*a} Mirosław Krawczyk,^a Ganna Maslak,^b Olga Abraimova^b and Martin Jönsson-Niedziółka ^{*a}

We present the formation of a cheap and environmentally friendly working electrode material for glucose biosensors with good catalytic properties. The classic electrode in such devices consists of a conductive material modified with the enzyme glucose oxidase. The working principle is the electrochemical detection of hydrogen peroxide as a product of the enzymatic transformation of glucose. As a base material, we offer manganese dioxide; it is a natural highly selective catalyst for the decomposition of H₂O₂ and is electrochemically deposited onto the surface of ITO. We approached the formation of MnO₂ films systematically. By changing parameters such as the deposition method, pH of the electrolyte, and the drying temperature of the precipitate, a series of electrodes were formed. These electrodes were characterized by SEM, electrochemical impedance spectroscopy, and XPS and their electrocatalytic activity was studied. Significant differences in the sensitivity of the electrodes were detected. The manganese dioxide film with the best catalytic characteristics is formed in the electrolyte with pH 1 by cyclic voltammetry and then drying at 60 °C. The surface of the electrode was then modified with a solution of GOx enzyme with a concentration of 2 mg ml⁻¹ (100–250 units per mg solid). The sensitivity of such an electrode is 117.8 μA mmol⁻¹ cm⁻². The range of determined concentrations of glucose is from 0.1 mM to 3 mM. The sensitivity is comparable to that of electrodes based on expensive materials such as graphene and noble metals.

Received 12th July 2023,
Accepted 21st August 2023
DOI: 10.1039/d3dt02199h

rsc.li/dalton

Introduction

The development of electrochemical biosensors has been an important area of biotechnology in recent times.^{1–4} Much of the work is devoted to the development of sensors for the determination of glucose.^{5–11} Today, most authors consider an increase in the sensitivity and high selectivity of the working electrodes of biosensors for glucose, the ability to analyse in a wide range of concentrations, and a low working potential to be important goals. The solution to such problems is often associated with the introduction of expensive materials such as graphene and carbon nanotubes, which increase the conductivity of the electrode material.^{12–14} Then the surface is modified with the enzyme glucose oxidase, which is an active,

highly stable, well studied and commercially available oxidoreductase.^{15,16} When using it, the principle of electrochemical detection of hydrogen peroxide as a product of the enzymatic transformation of the analyte (glucose) works.

MnO₂ is similar in catalytic properties to Pt, but its cost is much lower. In some publications, manganese dioxide was used as a natural highly selective catalyst for the decomposition of H₂O₂. The material is environmentally friendly and quite easily formed on the surface of the substrate. Particular attention is paid to its formation methods. Most researchers prefer time-consuming thermochemical or sol-gel techniques for the formation of dioxide.^{17–21} However, the formation of MnO₂ by electrochemical methods is a fast and easy process. There are a number of publications^{22–24} where electrochemically deposited MnO₂ was used as a catalyst, but the effect of the nature of the electrolyte, pH, electroplating technique and other conditions of film formation is not described. By changing deposition conditions such as the potential, concentration and pH of the electrolyte, it is easy to influence the structure and composition of thin films of MnO₂. The electrocatalytic activity of electrodes depends on these factors.²⁵

In this article we report the results of a study of the electrocatalytic activity towards decomposition of hydrogen peroxide

^aCharge Transfer in Hydrodynamic Systems group, Institute of Physical Chemistry of the Polish Academy of Sciences, Kasprzaka street 44/52, 01-224 Warsaw, Poland.

E-mail: vpoltavets@ichf.edu.pl, mkrawczyk@ichf.edu.pl, martinj@ichf.edu.pl

^bDepartment of Biochemistry and Medical Chemistry, Dnipro State Medical University, ul. Volodymyr Vernadsky 9, 49044 Dnipro, Ukraine.

E-mail: 205_04@dmu.edu.ua

† Electronic supplementary information (ESI) available: Additional XPS, XRD and SEM data. See DOI: <https://doi.org/10.1039/d3dt02199h>



of electrodes formed by MnO₂ electroplating at various pH from sulphate electrolytes on the surface of indium tin oxide coated glass (ITO) using several electrochemical techniques. The composition, morphology, and conductivity of the formed films were studied. Subsequently, the electrodes were modified with the enzyme glucose oxidase (GOx) and tested for their performance in determining glucose. The study was carried out with the aim of forming sensitive electrodes for biosensors for the determination of glucose and, by extension, other analytes based on the determination of H₂O₂ from oxidase-catalyzed reactions.

Experimental

Reagents and chemicals

All materials and chemicals were purchased commercially and used in the form in which they were received. Manganese sulphate and sodium sulphate for electrolyte preparation, glucose oxidase from *Aspergillus niger* (Type X-S, lyophilised powder, 100–250 units per mg solid, without added oxygen, CAS-no.: 9001-37-0), glutaraldehyde (GA), sodium dihydrogen phosphate dihydrate and sodium hydrogen phosphate dihydrate for the preparation of phosphate buffer (PB) (0.1 M, pH 7), glucose monohydrate, and hydrogen peroxide (30%) were supplied by Sigma Aldrich. Ultra-pure water (18.2 MΩ cm) from a Sartorius Arium Comfort I system was used to prepare the solutions. ITO coated glass was from BIOTAIN CRYSTAL CO with the following characteristics: resistance 6–8 Ohm sq⁻¹, thickness ~185 nm, and transmittance >84%.

Fabrication of MnO₂ films on the surface of ITO

Glass substrates were sonicated for 20 min in acetone, then in ethanol, washed with deionized water and dried with Ar stream. A working area of 0.6940 cm² of the electrode was defined using a hole laser cut in Kapton tape. The electrochemical formation of the electrodes was carried out by the methods of cyclic voltammetry (CV) and chronoamperometry (CA) with time control. As electrolytes, we used water solutions of 0.005 M MnSO₄ and 0.5 M Na₂SO₄ with pH 1, pH 2, and pH 3.5, adjusted using H₂SO₄. All electrochemical experiments were performed using a potentiostat/galvanostat Bio-Logic SAS, model SP-300, s/n: 0582 in a conventional three-electrode glass cell. Ag/AgCl/3 M KCl was used as a reference and a Pt net as a counter electrode. Each potential reported in this paper is given against Ag/AgCl/3 M KCl at a laboratory temperature of 25 ± 1 °C.

With the CV method, the region of scanned potentials was selected depending on the pH of the electrolyte: for pH 1, from 0.65 V to 2.1 V; for pH 2, from 0.4 V to 1.7 V; and for pH 3.5, from 0.3 V to 1.4 V. The scan rate is 50 mV s⁻¹. With the CA method, the applied potential also varied with pH: for pH 1 – 2.0 V, for pH 2 – 1.7 V, and for pH 3.5 – 1.4 V. The deposition time was 200 s.

After electrodeposition the dioxide films were dried at 60 °C or 90 °C in air for 15 h.

Analytical procedures for determination of H₂O₂ and glucose concentration

The electrochemical measurements were all carried out at room temperature. The cyclic voltammograms of the MnO₂/ITO electrode were scanned from 0.3 to 0.9 V in 0.1 M PB. The scan rate was 100 mV s⁻¹.

The catalytic activity of the MnO₂/ITO electrodes was determined using chronoamperometry in 0.1 M PB. The amperometric response was measured at an applied potential of 0.45 V during repeated injections of 1 mM hydrogen peroxide.

For the determination of glucose, the electrode was modified by adding 2 μl of 1 mg ml⁻¹, 2 mg ml⁻¹, 3 mg ml⁻¹ or 4 mg ml⁻¹ GOx solutions. Then the electrode was placed in a closed container over a concentrated GA solution (25%) and kept there at room temperature for 7 minutes. Thus, we fixed the enzyme on the surface of manganese dioxide.

The catalytic activity of the GOx/MnO₂/ITO material was measured by CA in 0.1 M PB. The amperometric response was measured at an applied potential of 0.45 V during injections of 1 mM or 0.1 mM glucose.

Physical characterization of MnO₂/ITO electrodes

The microstructure and morphology of the MnO₂/ITO samples were investigated using an FEI Nova NanoSEM 450 scanning electron microscope.

Electrochemical impedance spectroscopy (EIS) was performed in 5 mM [Fe(CN)₆]^{3-/4-} in the frequency range of 0.25 to 100 000 Hz with an amplitude of 5 mV.

X-ray photoelectron spectroscopy (XPS) measurements were performed using a PHI 5000 VersaProbe (ULVAC-PHI) spectrometer with monochromatic Al Kα radiation (*h* = 1486.6 eV) from an X-ray source operating at 100 μm spot size, 25 W and 15 kV. High-resolution (HR) XPS spectra were collected with a hemispherical analyzer at a pass energy of 117.4 and an energy step size of 0.1 eV. The X-ray beam was incident at the sample surface at an angle of 45° with respect to the surface normal, and the analyzer axis was located at 45° with respect to the surface. CasaXPS software was used to evaluate the XPS data. Deconvolution of all HR XPS spectra was performed using a Shirley background and a Gaussian peak shape with 30% Lorentzian character. The measured binding energies (BE) for individual elements were corrected in relation to the C1s carbon peak at 284.8 eV.

Results and discussion

Electrodeposition of MnO₂ on ITO

To investigate the formation of MnO₂/ITO electrodes we performed the electrodeposition at different pH and used two methods of electroplating. In fact, we were quite limited in choosing the pH of the solution. On the one hand, we can't use electrolytes with pH less than 1, because then the electrodeposition of MnO₂ is accompanied by parallel evolution of oxygen. As a result, the precipitate is removed from the surface of the electrode by gas bubbles. On the other hand, at a pH



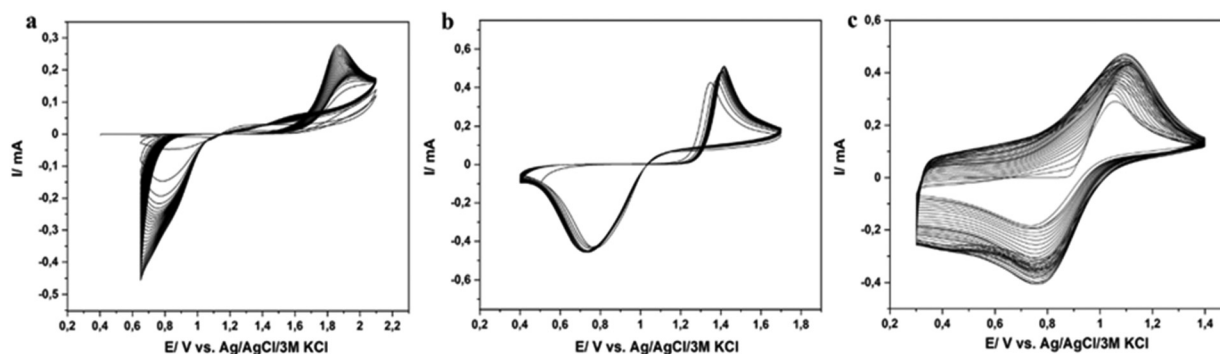
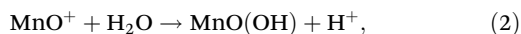
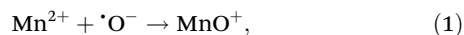


Fig. 1 Electrodeposition of MnO_2 by the CV method from a water solution of 0.005 M MnSO_4 + 0.5 M Na_2SO_4 electrolyte (a) at pH 1, (b) at pH 2, and (c) at pH 3.5. Scan rate was 50 mV s^{-1} .

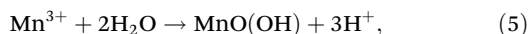
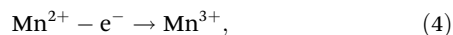
value close to neutral and alkaline values, the oxide forms of manganese precipitate. Therefore, in this work, we use solutions at pH 1, 2 and 3.5. Fig. 1 shows the dependencies obtained during the formation of the precipitate by the CV method.

With this method the precipitate is deposited and partly dissolved cyclically, and thus active centers are formed and the sediment builds up around these. It should be noted that the potential for the start of the reaction shifts depending on the pH of the electrolyte. As the pH value increases, the potential for the start of the anodic reaction shifts significantly to less positive values. As suggested in ref. 26, this may be due to the predominance of the chemical pathway of Mn^{2+} ion oxidation in less acidic electrolytes. The competing pathways of reactions are as follows:

at $E < E^\circ (\text{Mn}^{2+}/\text{Mn}^{3+})$



at $E > E^\circ (\text{Mn}^{2+}/\text{Mn}^{3+})$



with further oxidation of $\text{MnO}(\text{OH})$ to MnO_2 by reaction (3), where $[\text{O}]^*$ represents an available oxidation agent. According to both mechanisms, one of the intermediates is $\text{MnO}(\text{OH})$, and the subsequent chemical oxidation is a slow reaction step, and, therefore, the presence of $\text{MnO}(\text{OH})$ in the precipitate is expected.

Some electrodes with MnO_2/ITO were formed by the classical method of CA at a constant applied potential. The potential was selected depending on the pH of the solution on the basis of CV measurements. Also, we controlled the time to obtain thin films. At the given concentration of Mn^{2+} ions, precipitation was found to be optimal after 200 s. As a result, thin films of MnO_2 are formed, which have sufficient conductivity

and mechanical strength. MnO_2 is known for its poor conductivity, so thicker films block electron transfer.

Drying is an important part of electrode formation. The drying temperature can have a strong effect on the composition, structure and catalytic properties of such a complex system as anodic deposited manganese dioxide. The precipitates were dried in air at 60°C and 90°C . Temperatures above 100°C are not recommended, as a large amount of water in the sediment boils and cracks the film. After drying, manganese dioxide shows good mechanical properties and affinity for the surface.

Thus, 12 sets of electrodes were formed under conditions combining the pH of the electrolyte, the precipitation method and the drying temperature. The symbols of the electrodes that we use in the remaining text of the article and the features of their formation are shown in Table 1.

Characteristics of MnO_2/ITO electrodes

XPS measurements were employed to test the influence of the electrolyte pH and the drying temperature on the composition of Mn oxides in films. We also have checked for the presence of the characteristic compound $\text{MnO}(\text{OH})$ in the precipitates. The results are shown in Fig. 2.

The spectra in Fig. 2a and b are the results of the analysis of the film electrodeposited on ITO at pH 1 by the CV method

Table 1 Description and naming of the electrodes investigated

Name of electrode	pH of electrolyte	Method of deposition	Drying temperature, $^\circ\text{C}$
pH1_CV_60	1	CV	60
pH1_CA_60	1	CA	60
pH1_CV_90	1	CV	90
pH1_CA_90	1	CA	90
pH2_CV_60	2	CV	60
pH2_CA_60	2	CA	60
pH2_CV_90	2	CV	90
pH2_CA_90	2	CA	90
pH3.5_CV_60	3.5	CV	60
pH3.5_CA_60	3.5	CA	60
pH3.5_CV_90	3.5	CV	90
pH3.5_CA_90	3.5	CA	90



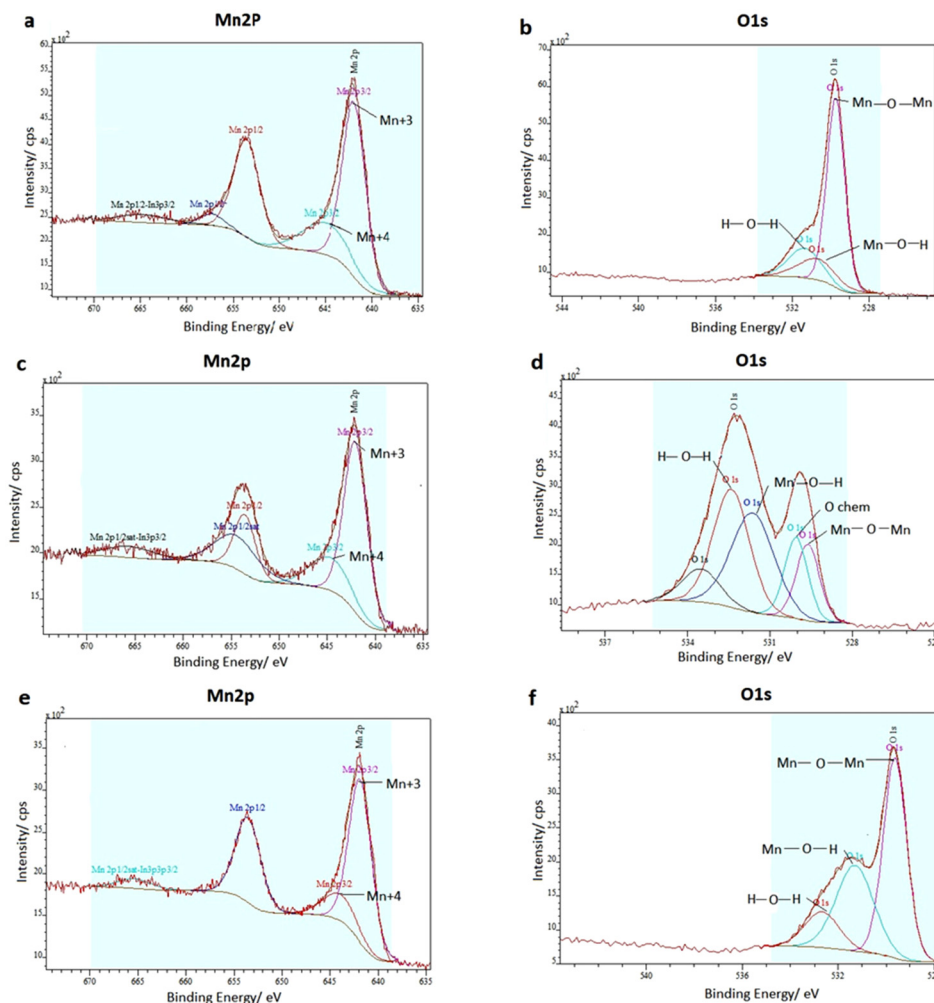


Fig. 2 Mn 2p and O1s XPS spectra of (a and b) pH1_CV_60, (c and d) pH1_CV_90, and (e and f) pH3.5_CV_60. For details, see the main text.

(30 cycles) and dried at 60 °C. The Mn 2p spectrum contains Mn 2p_{3/2} and Mn 2p_{1/2} signals located at 641.84 eV and 653.55 eV, respectively, with a spin energy separation of 11.7 eV corresponding to a mixture of oxides which all are described by the formal name MnO₂.^{27–29} According to previous reports, the Mn 2p_{3/2} spectrum exhibits pairs of peaks located at 641.93 eV and 644.90 eV, corresponding to the Mn³⁺ and Mn⁴⁺ species in the heterostructure.^{30,31} The trivalent and tetravalent manganese species are in ratios of 67.91% and 32.09%. The O1s spectrum gives important information about the forms of manganese oxides and the presence of hydrolyzed

forms of manganese. We can identify the Mn–O–Mn bond at 529.63 eV (65.53%) for tetravalent oxide, the Mn–O–H bond at 531.3 eV (18.62%) for hydrated trivalent oxide and the H–O–H bond at 532.68 eV (15.85%) for water.^{32,33}

The spectra in Fig. 2c–f were analysed in a similar way and the results are summarized in Table 2. Noteworthy is the appearance of chemical oxygen as the peak at 530.03 eV (14.02%) in Fig. 2d (pH1_CV_90).

Comparison of the results suggests that the pH of electrolyte significantly affects the composition of the formed film. In a more acidic environment the precipitate with a high percen-

Table 2 XPS spectra interpretation

The conditions of formation	Mn 2p spectrum, spin energy separation, eV	Mn ³⁺ , %	Mn ⁴⁺ , %	Mn–O–Mn, %	Mn–O–H, %	H–O–H, %	O _{chem} , %
pH 1, CV method, drying at 60 °C	11.7	67.90	32.09	65.53	18.62	15.85	—
pH 1, CV method, drying at 90 °C	11.6	81.54	18.46	13.32	31.74	31.90	14.02
pH 3.5, CV method, drying at 60 °C	11.7	72.77	27.23	51.42	35.05	13.53	—



tage of Mn^{4+} is deposited. This film contains the hydrolyzed form $\text{MnO}(\text{OH})$, but in a smaller amount compared to other samples. This is explained by the inhibition of hydrolysis at pH 1. The composition of the film deposited under the same conditions but dried at a higher temperature changed significantly. We found a higher concentration of Mn^{3+} and a significant increase in the concentration of hydrolyzed particles. It is likely that this effect is achieved due to the presence of Mn^{2+} particles adsorbed on the surface of the deposit during the electrodeposition process. They interact with Mn^{4+} and form $\text{MnO}(\text{OH})$ according to reaction (6).³¹



Raising the temperature promotes an increase in the rate of reaction and the rate of hydrolysis. Predictably, we find a significant amount of the hydrolyzed form $\text{MnO}(\text{OH})$ in the precipitate formed at pH 3.5. A more alkaline environment is favorable for hydrolysis processes.

The results of the XPS analysis were supported by the EIS data. The measurements were performed in order to further explore the charge transfer through the film. The plots are shown in Fig. 3. The equivalent circuit model $R_1 + Q_2/(R_2 + W_2)$ was employed to analyse the EIS data, where R_1 is the uncompensated resistance, R_2 is the charge-transfer resistance, Q is the constant phase element and W is the Warburg element.

The analysis of dependencies in Fig. 3 is presented in Table 3.

Comparison of the data shows the least charge-transfer resistance for films precipitated by the CV method and dried at

60 °C. An increased drying temperature and the chronoamperometry precipitation method seem to lead to a higher content of $\text{MnO}(\text{OH})$ – this phase is known for its poor conductivity.

The morphologies of all sediments were studied by scanning electron microscopy. Fig. 4 shows the images of MnO_2 films deposited from sulfate electrolytes with different pH. The samples were prepared *via* CV and CA methods. Additional SEM images are found in the ESI.†

The first conclusion from Fig. 4 – the pH of the solution and the method of precipitation have a huge impact on the morphology of the electrodeposited manganese dioxide. Images 1–6, 11–14, and 19–22 (Fig. 4) show the surface of the sediments deposited by the CV method. With this technique the precipitate is formed and partially dissolved, thus forming active centers. In subsequent cycles the sediment builds up around these centers. As a result, the MnO_2 films form branching networks which provide an extra-large surface area. The precipitates formed at pH 1 can be seen in the images 1–6 (Fig. 4). They are uniform and we could control their thickness by the number of deposition/dissolution cycles. The film formed during 30 cycles is ultra-thin; the highly conductive ITO can be seen through the deposit. At pH 2 (images 11–14 in Fig. 4), the precipitates are quite dense and not very branched, and when heated, they crack. A special precipitate is observed during precipitation from an electrolyte with pH 3.5 (images 19–22 in Fig. 4). The sediment is porous and looks like a sponge, but there is spreading, which can be associated with the presence of hydrolyzed forms in the composition. The precipitates formed by the CA method are shown in images 7–10, 15–18, and 23–26 (Fig. 4). They have a denser structure and we can sometimes see cracks formed in the film. It is worth paying attention to the sediment formed in the electrolyte with pH 1 by the CA method (images 9 and 10 in Fig. 4). When drying at 90 °C, dense spherical shapes are formed. This may indicate a slow chemical reaction taking place after the precipitation, which changes the precipitate composition and, as a result, the sediment morphology.

XRD studies of the precipitates obtained were carried out, but no clear peaks characteristic of manganese dioxide were observed. The spectra are given in the ESI.† We concluded that we obtained amorphous structures of MnO_2 .

Summarizing the results of all physicochemical studies, the following conclusions can be made. Electrochemically produced films of manganese dioxide contain a significant amount of water, despite prolonged drying. Significant influence of the pH of the electrolyte on the sediment composition is observed. With an increase in the acidity of the solution, the proportion of Mn^{4+} increases, and the content of the hydro-

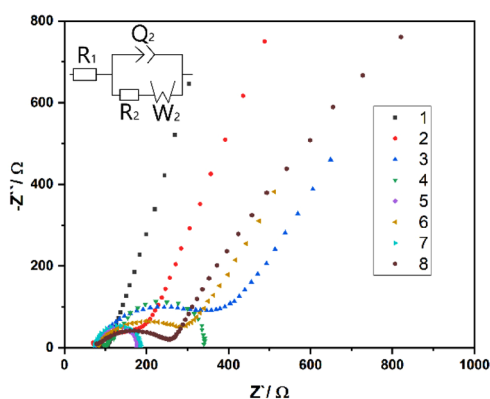


Fig. 3 Electrochemical impedance spectroscopy was performed on (1) pH1_CV_60 (30 cycles), (2) pH1_CV_60 (40 cycles), (3) pH1_CV_90, (4) pH1_CA_60, (5) pH2_CV_60, (6) pH2_CA_60, (7) pH3.5_CV_60, and (8) pH3.5_CA_60. For details, see the main text.

Table 3 The values of charge-transfer resistance, R_2 , for the corresponding precipitation in Fig. 3

Electrode	pH 1_CV_60 (30 cycles)	pH 1_CV_60 (40 cycles)	pH 1_CV_90	pH 1_CA_60	pH 2_CV_60	pH 2_CA_60	pH 3.5_CV_60	pH 3.5_CA_60
R_2 , Ohm	87.11	136.9	245.9	229.9	100.6	177.6	112.4	209.9



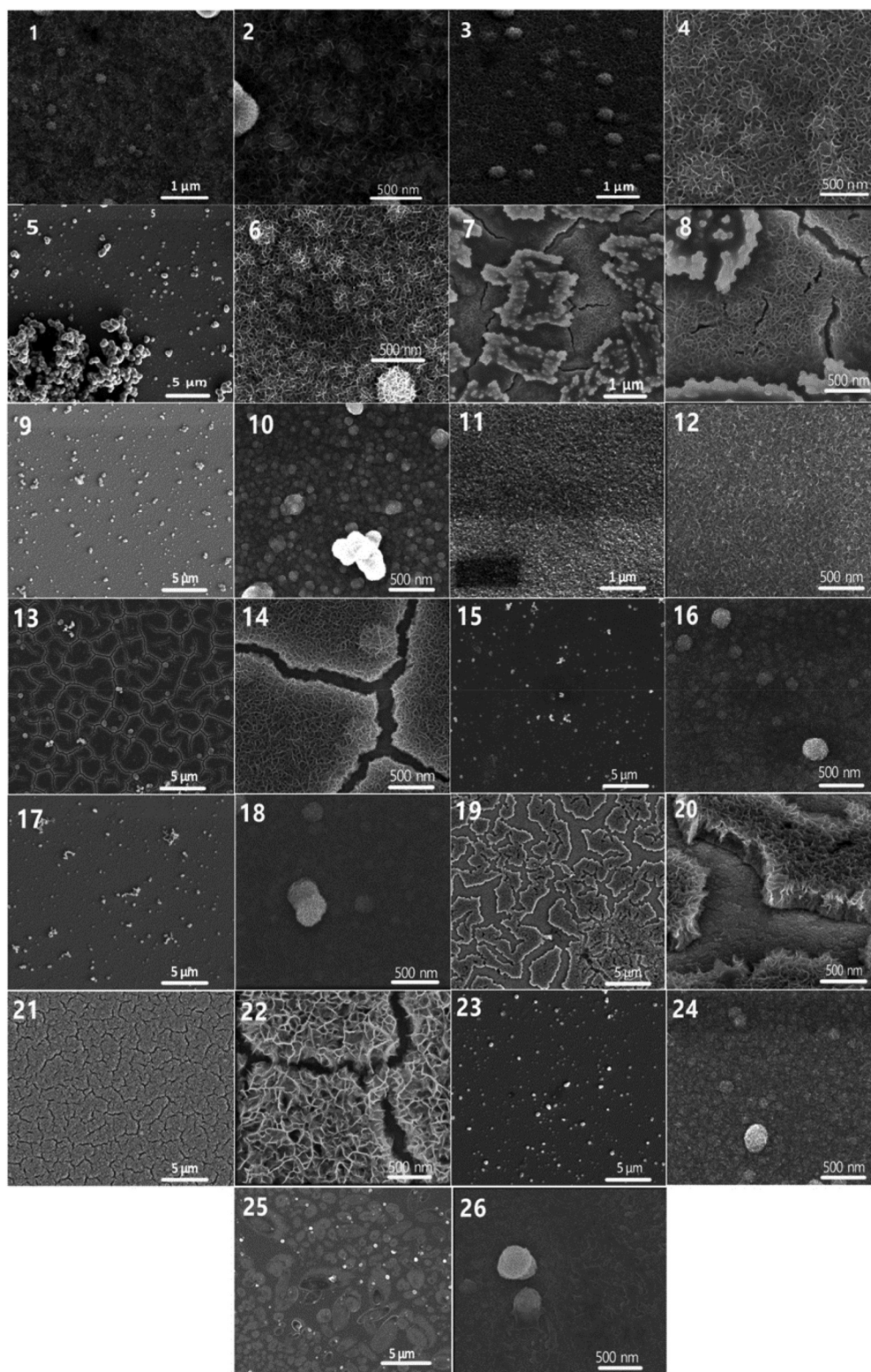


Fig. 4 SEM images of MnO_2 films deposited under the following conditions: (1, 2) pH1_CV_60 (30 cycles), (3, 4) pH1_CV_60 (40 cycles), (5, 6) pH1_CV_90, (7, 8) pH1_CA_60, (9, 10) pH1_CA_90, (11, 12) pH2_CV_60, (13, 14) pH2_CV_90, (15, 16) pH2_CA_60, (17, 18) pH2_CA_90, (19, 20) pH3.5_CV_60, (21, 22) pH3.5_CV_90, (23, 24) pH3.5_CA_60, and (25, 26) pH3.5_CA_90. For details, see the main text.



lyzed form of trivalent manganese $\text{MnO}(\text{OH})$ decreases. This affects the conductivity, as we find that a precipitate from a more acidic solution shows better conductivity. However, the absolute values of charge-transfer resistance remain significant.

A slight increase in drying temperature activates an internal reaction and leads to an increase in the content of $\text{MnO}(\text{OH})$. It is possible that a further increase in the drying temperature of the precipitates could lead to additional oxidation of Mn^{3+} , but temperatures above 100 °C would lead to mechanical degradation of the film.

Keeping the drying temperature lower had a positive effect on the mechanical strength of the resulting films. Thus, we obtained uniform precipitation without cracks and with a branched structure and places for further accommodation of enzyme molecules.

In the next section, we will see which of these characteristics have an effect on the catalytic activity of manganese dioxide.

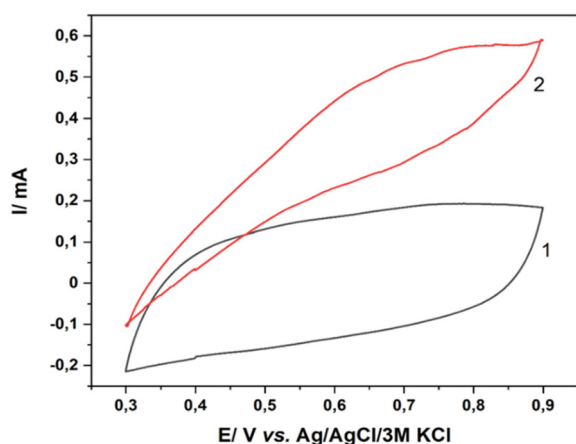


Fig. 5 CVs of bare MnO_2 in the absence (1) and presence (2) of 2 mM H_2O_2 in PB water solution. Scan rate was 100 mV s^{-1} .

Analytical procedure for the determination of H_2O_2 and glucose

The catalytic properties of the formed MnO_2/ITO electrodes were tested in the process of electrocatalytic decomposition of hydrogen peroxide. Based on data from the literature^{34,35} the mechanism of the process of electrochemical determination of H_2O_2 is as follows. During the catalytic decomposition of hydrogen peroxide in the presence of MnO_2 , Mn^{4+} is reduced to Mn^{3+} , and possibly even to Mn^{2+} . However, when anodic polarization is applied to the electrode, the reverse oxidation of Mn^{3+} to Mn^{4+} occurs. From the value of the recorded anode current we can quantitatively determine the decomposed H_2O_2 . The electrochemical properties of the developed electrodes were first characterized by cyclic voltammetry in 0.1 M PB (pH 7) at a scan rate of 100 mV s^{-1} in the potential range from 0.3 V to 0.9 V vs. Ag/AgCl/3 M KCl. The dependence obtained on the electrode pH1_CV_60 is shown in Fig. 5. The voltammogram 1 without visible peaks was recorded in an electrolyte free of peroxide. The voltammogram 2 reflects the currents recorded in the presence of 2 mM H_2O_2 added to the electrolyte. We note an increase in current by 0.1–0.5 mA in the presence of peroxide, and the maximum value of 0.55 mA is reached at a potential of 0.8 V vs. Ag/AgCl/3 M KCl. Such data indicate a high catalytic activity of the electrode for this process.

The MnO_2/ITO electrodes' sensing properties were also investigated by chronoamperometry at an applied anodic potential. After a series of tests (data not shown), where sufficient sensitivity of the electrode without too much noise was evaluated, we were convinced that the most appropriate potential is +0.45 V vs. Ag/AgCl/3 M KCl.

The chronoamperometric responses upon addition of hydrogen peroxide and later glucose, at selected working potentials, show staircase-like signals with most examined electrodes. Fig. 6 illustrates the amperometric responses of MnO_2/ITO electrodes deposited under different conditions (a complete description of the formation of 12 electrodes is given in Table 1.) upon injection of H_2O_2 so that each injection changes the concentration in the cell by 1 mM.

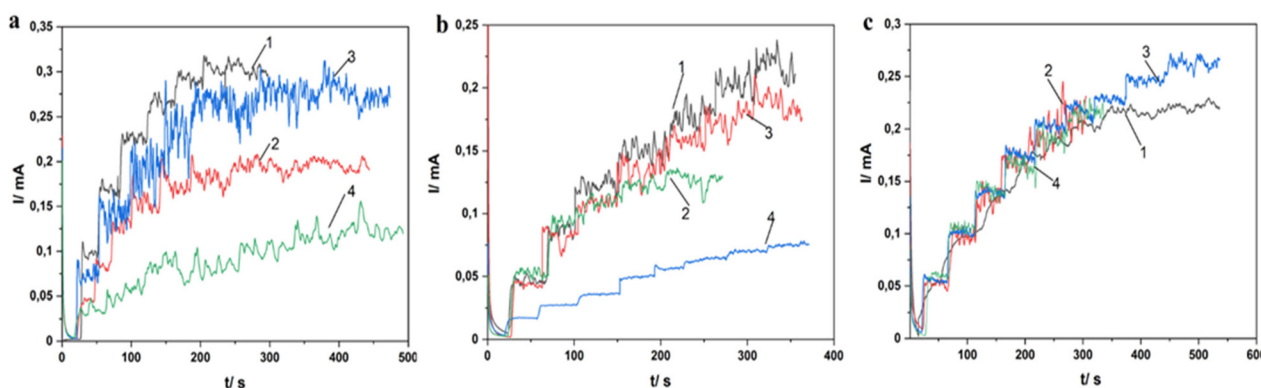


Fig. 6 Typical amperometric $i-t$ curves upon successive injection of H_2O_2 (1 mM) into stirring PB at an applied potential of 0.45 V vs. Ag/AgCl/3 M KCl of MnO_2/ITO electrodes: (a1) pH1_CV_60, (a2) pH1_CA_60, (a3) pH1_CV_90, (a4) pH1_CA_90, (b1) pH2_CV_60, (b2) pH2_CA_60, (b3) pH2_CV_90, (b4) pH2_CA_90, (c1) pH3.5_CV_60, (c2) pH3.5_CA_60, (c3) pH3.5_CV_90, and (c4) pH3.5_CA_90. Note that the vertical scales are different.



For clarity, the test results of the electrodes are divided into 3 images: Fig. 6a – the electrodes were formed in the electrolyte with pH 1; Fig. 6b – the electrodes were formed in the electrolyte with pH 2; Fig. 6c – the electrodes were formed in the electrolyte with pH 3.5. The time for reaching the steady-state current for all electrodes varies from 5 to 50 seconds. In Fig. 6a and b we note a significant influence of the deposition method on the sensitivity of the electrode (the value of the detected current). In these cases the electrodes deposited by the CA method show the lowest sensitivity. The success of the CV method can be explained by the large surface area of the synthesized material. One can also see the effect of the drying temperature of the samples. High sensitivity is shown by electrodes dried at 60 °C. For some of the electrodes, the response is very noisy, especially at higher concentrations of H₂O₂. The dependence of sensitivity on the deposition method and drying temperature of the electrodes is not observed in Fig. 6c,

showing that deposition at pH 3.5 gives consistent results relatively independent of the method.

Fig. 7 shows the dependence of the current on the concentration of H₂O₂ up to 6 mM. It should be noted that such a dependence is linear at low concentrations, and as the sensitivity decreases, linearity appears in a larger concentration range. The best result was shown by the precipitate formed in the electrolyte at pH 1 by the CV method and then dried at 60 °C for 15 hours. However, at H₂O₂ concentrations above 3 mM, a dependence similar to Michaelis Menten dependence is observed. This can be explained by contamination of the electrode surface with reaction products or by changes in the composition and morphology as a result of constant reverse oxidation and reduction reactions of manganese dioxide during the electrocatalytic processes.

Summarizing the intermediate results of the catalysis of hydrogen peroxide decomposition, we observe that the best response is demonstrated by electrodes where the MnO₂ films are deposited in an electrolyte with pH 1 (Fig. 6 and 7). This means, according to the XPS data, that a higher proportion of Mn⁴⁺ increases their catalytic properties. The method of deposition also affects, and CV gives a branched structure, which provides a large surface area of contact with hydrogen peroxide. As a result, the catalytic activity of the electrode increases.

All twelve samples of manganese dioxide electrodes were modified by the addition of GOx enzyme solution (1 mg ml⁻¹) and fixed by GA, which is used as a cross-linking agent for enzymes.^{36–38} Bonding occurs at amino groups and thus, enzyme molecules are fixed on the surface and are not washed off by the electrolyte. The amperometric responses upon injection of aliquots that increase the concentration in steps of 1 mM glucose were investigated and the obtained amperograms are shown in Fig. 8.

As in the study of catalysis of hydrogen peroxide decomposition, the *i*-*t* dependences were divided into three figures according to the same principle. The time for reaching the steady-state current for all electrodes is not more than 5 seconds. When the surface of electrodes was modified with

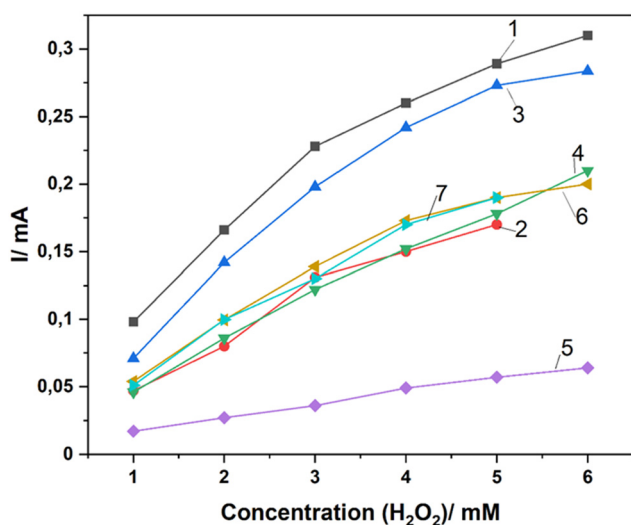


Fig. 7 Relationship of the amperometric response vs. the H₂O₂ concentration: (1) pH1_CV_60, (2) pH1_CA_60, (3) pH1_CV_90, (4) pH2_CV_60, (5) pH2_CV_90, (6) pH3.5_CV_60, and (7) pH3.5_CA_60.

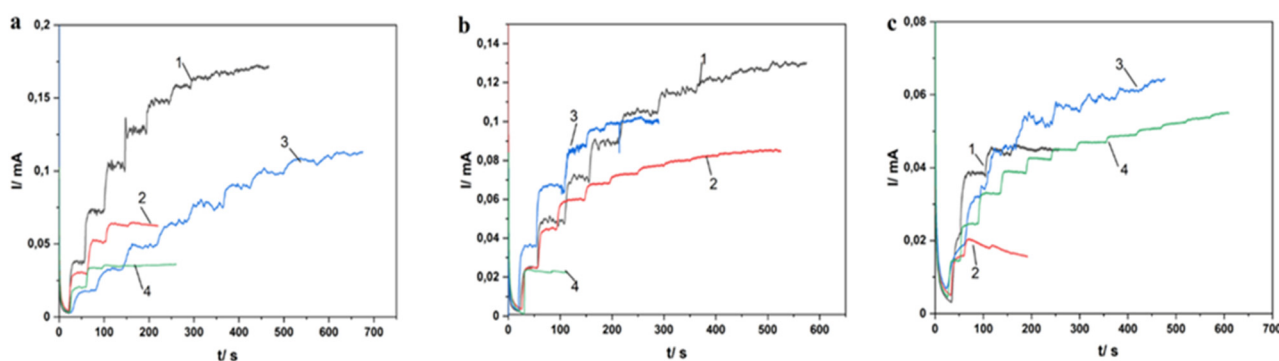


Fig. 8 Typical amperometric *i*-*t* curves on successive injection of glucose (1 mM) into stirring PB at an applied potential of 0.45 V vs. Ag/AgCl/3 M KCl of modified MnO₂ electrodes: (a1) pH1_CV_60, (a2) pH1_CA_60, (a3) pH1_CV_90, (a4) pH1_CA_90, (b1) pH2_CV_60, (b2) pH2_CA_60, (b3) pH2_CV_90, (b4) pH2_CA_90, (c1) pH3.5_CV_60, (c2) pH3.5_CA_60, (c3) pH3.5_CV_90, and (c4) pH3.5_CA_90. Note that the vertical scales are different.



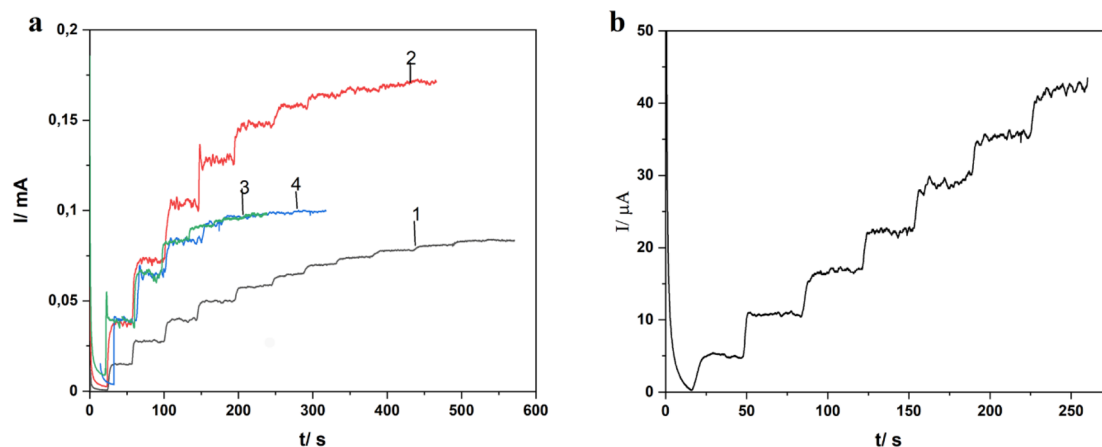


Fig. 9 Amperometric $i-t$ curves on successive injection of glucose into stirring PB at an applied potential of 0.45 V (a) of MnO_2/ITO electrodes modified by adding glucose oxidase solution: (1) 1 mg ml^{-1} , (2) 2 mg ml^{-1} , (3) 3 mg ml^{-1} , and (4) 4 mg ml^{-1} (injection 1 mM); (b) MnO_2/ITO , modified by glucose oxidase solution (2 mg ml^{-1}) (injection 0.1 mM).

enzyme molecules, the surface morphology began to play an even more significant role. The most active electrodes are those where manganese dioxide is deposited cyclically with partial dissolution. Based on SEM images, the CV method provides a branched structure in which the enzyme molecules can be intercalated. On the other hand, a correlation between the catalytic activity of manganese dioxide and electrodes modified with the

enzyme was observed. This makes it possible to use the simple and cheap response of hydrogen peroxide to test the biocatalytic properties of the electrodes on the basis of MnO_2 .

The best analytical parameters were obtained for the electrode formed in the electrolyte with pH 1 by the CV method and dried at 60°C . It shows the best catalytic and mechanical properties. To improve the sensitivity of the electrode, we increased the enzyme content on its surface by the increasing the concentration of the enzyme in solutions that modified the electrodes. The optimal concentration of the enzyme is 2 mg ml^{-1} (Fig. 9). At higher enzyme concentrations, steric hindrance may be involved and results worsened. The calibration curve obtained for glucose in PB buffer at a potential of 0.45 V vs. Ag/AgCl/3 M KCl is shown in Fig. 9. The chronoamperometric current response upon injection of aliquots that increase the concentration in steps of 0.1 mM glucose shows linear dependence and it can be expressed with a correlation coefficient of $R^2 = 0.998$.

Using the data of dependence 2 (Fig. 9a) and dependence in Fig. 9b, a calibration curve (Fig. 10) was generated with the maximum range of possible determined concentrations.

The GOx/ MnO_2/ITO electrode shows a linear relationship with the concentration of H_2O_2 ranging from 0.1 mM to 3 mM with a correlation coefficient of 0.9938.

The characteristics of the developed electrode were compared with some recently reported literature data, and the results are presented in Table 4.

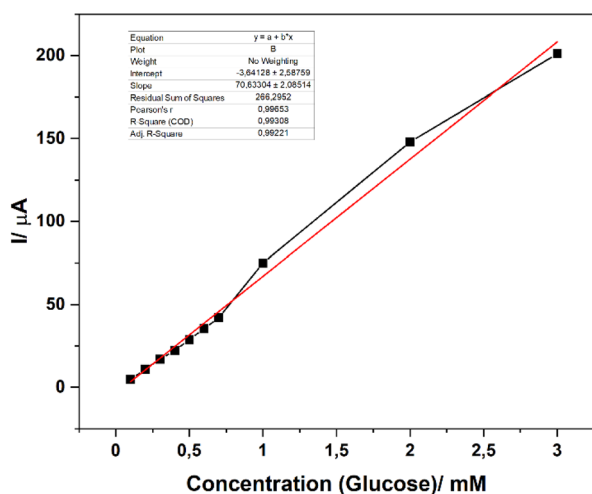


Fig. 10 Calibration plot of electrocatalytic current versus glucose concentration.

Table 4 Comparison of the electrocatalytic performance of GOx/ MnO_2/ITO with that of other enzymatic glucose sensors

Electrode	Measurement technique	Applied potential, V	Range, mM	Sensitivity, $\mu\text{A mmol}^{-1} \text{ cm}^{-2}$	Ref.
PPy-Gox/PPy-Cl	CA	+0.7	0.5–24.0	3.5	39
Gox/AuNPs/BSA/ Fe_3O_2	CA	+0.4	0.25–7.0	115.3	40
Gox/Naf/ MnO_2/GCE	CA	+0.7	0.2–2.8	38.2	41
Gox/Naf/ $\text{MnO}_2/\text{GNR}/\text{GCE}$	CA	+0.5	0.1–1.4	56.32	42
Ch.m-Gox-PB/conductor	CA	0	1–20	17	43
Gox/ MnO_2/ITO	CA	+0.45	0.1–3.0	117.8	Our paper



Our GOx/MnO₂/ITO electrode was compared in terms of characteristics such as sensitivity and the range of determined concentrations. The sensitivity of the electrode is comparable only to that of the sample based on Au nanoparticles.⁴⁰ It was interesting to compare our developed electrode with the electrode of glucose biosensors based on a Prussian blue catalyst.⁴³ We note a wide range of analyte determination, but the detection limit is rather high and such a biosensor cannot be used in all areas of science. The range of possible determination of the concentration of glucose is comparable to that of an electrode based on graphene.⁴² Graphene and noble metals are quite expensive materials. The developed electrode with similar characteristics is much cheaper and is easily formed.

Conclusion

The use of MnO₂ in the development of electrodes intended for biosensors for the enzymatic determination of glucose is very promising. This material exhibits a high electrocatalytic activity in hydrogen peroxide decomposition, which is released during enzymatic oxidation of glucose. In this paper we show that manganese dioxide film properties depend on the composition and surface area of the material. We found a tendency of increased catalytic properties during precipitation in a more acidic electrolyte, which is associated with the predominance of the phase Mn⁴⁺. An easy-to-implement CV method was also used to deposit a film of manganese dioxide, which gave a branched structure with a larger surface area. This enhanced the catalytic properties of the precipitate. The film MnO₂, electroplated under suitable conditions, shows electrocatalytic activity comparable with that of electrodes based on graphene and gold nanoparticles. The electrochemical formation of oxide films is an easy, fast, reproducible and effective method. The manganese dioxide film with better characteristics is formed electrochemically on the surface of ITO in electrolyte with pH 1 by the CV method and then drying at 60 °C. The maximum efficiency of electrode GOx/MnO₂/ITO appears after modification with a solution of GOx enzyme with a concentration of 2 mg ml⁻¹. The sensitivity of such an electrode is 117.8 μA mmol⁻¹ cm⁻². The developed electrode can be used in glucose biosensors or similar systems.

Conflicts of interest

There are no conflicts to declare.

Acknowledgements

This work was supported by the Norway Grants 2014-2021 via the National Centre for Research and Development (NOR/POLNOR/UPTURN-UA/0060/2019).

References

- 1 M. Bäcker, D. Rakowski, A. Poghossian, M. Biselli, P. Wagner and M. J. Schöning, Chip-Based Amperometric Enzyme Sensor System for Monitoring of Bioprocesses by Flow-Injection, Analysis, *J. Biotechnol.*, 2013, **163**(4), 371–376, DOI: [10.1016/j.jbiotec.2012.03.014](https://doi.org/10.1016/j.jbiotec.2012.03.014).
- 2 L. Xue, N. Jin, R. Guo, S. Wang, W. Qi, Y. Li and J. Lin, Microfluidic Colorimetric Biosensors Based on MnO₂ Nanozymes and Convergence–Divergence Spiral Micromixers for Rapid and Sensitive Detection of Salmonella, *ACS Sens.*, 2021, **6**(8), 2883–2892, DOI: [10.1021/acssensors.1c00292](https://doi.org/10.1021/acssensors.1c00292).
- 3 R. Bi, X. Ma, K. Miao, P. Ma and Q. Wang, Enzymatic Biosensor Based on Dendritic Gold Nanostructure and Enzyme Precipitation Coating for Glucose Sensing and Detection, *Enzyme Microb. Technol.*, 2023, **162**, 110132, DOI: [10.1016/j.enzmictec.2022.110132](https://doi.org/10.1016/j.enzmictec.2022.110132).
- 4 J. Kim, A. S. Campbell, B. E.-F. de Ávila and J. Wang, Wearable Biosensors for Healthcare Monitoring, *Nat. Biotechnol.*, 2019, **37**(4), 389–406, DOI: [10.1038/s41587-019-0045-y](https://doi.org/10.1038/s41587-019-0045-y).
- 5 E. Witkowska Nery, M. Kundys, P. S. Jeleń and M. Jönsson-Niedziółka, Electrochemical Glucose Sensing: Is There Still Room for Improvement?, *Anal. Chem.*, 2016, **88**(23), 11271–11282, DOI: [10.1021/acs.analchem.6b03151](https://doi.org/10.1021/acs.analchem.6b03151).
- 6 W.-Y. Jeon, H.-H. Kim and Y.-B. Choi, Development of a Glucose Sensor Based on Glucose Dehydrogenase Using Polydopamine-Functionalized Nanotubes, *Membranes*, 2021, **11**(6), 384, DOI: [10.3390/membranes11060384](https://doi.org/10.3390/membranes11060384).
- 7 L. Wang, X. Gao, L. Jin, Q. Wu, Z. Chen and X. Lin, Amperometric Glucose Biosensor Based on Silver Nanowires and Glucose Oxidase, *Sens. Actuators, B*, 2013, **176**, 9–14, DOI: [10.1016/j.snb.2012.08.077](https://doi.org/10.1016/j.snb.2012.08.077).
- 8 H. Jia, N. Shang, Y. Feng, H. Ye, J. Zhao, H. Wang, C. Wang and Y. Zhang, Facile preparation of Ni nanoparticle embedded on mesoporous carbon nanorods for non-enzymatic glucose detection, *J. Colloid Interface Sci.*, 2021, **583**, 310–320, DOI: [10.1016/j.jcis.2020.09.051](https://doi.org/10.1016/j.jcis.2020.09.051).
- 9 S. An, N. Shang, B. Chen, Y. Kang, M. Su, C. Wang and Y. Zhang, Co-Ni layered double hydroxides wrapped on leaf-shaped copper oxide hybrids for non-enzymatic detection of glucose, *J. Colloid Interface Sci.*, 2021, **592**, 205–214, DOI: [10.1016/j.jcis.2021.02.046](https://doi.org/10.1016/j.jcis.2021.02.046).
- 10 T. Meng, N. Shang, J. Zhao, M. Su, C. Wang and Y. Zhang, Facile one-pot synthesis of Co coordination polymer spheres doped macroporous carbon and its application for electrocatalytic oxidation of glucose, *J. Colloid Interface Sci.*, 2021, **589**, 135–146, DOI: [10.1016/j.jcis.2020.12.119](https://doi.org/10.1016/j.jcis.2020.12.119).
- 11 S. De Zio, M. Beconi, A. Soldà, M. Malferrari, A. Lesch and S. Rapino, Glucose Micro-Biosensor for Scanning Electrochemical Microscopy Characterization of Cellular Metabolism in Hypoxic Microenvironments, *Bioelectrochemistry*, 2023, **150**, 108343, DOI: [10.1016/j.bioelechem.2022.108343](https://doi.org/10.1016/j.bioelechem.2022.108343).
- 12 L. Hao, S.-S. Li, J. Wang, Y. Tan, L. Bai and A. Liu, MnO₂/Multi-Walled Carbon Nanotubes Based Nanocomposite



- with Enhanced Electrocatalytic Activity for Sensitive Amperometric Glucose Biosensing, *J. Electroanal. Chem.*, 2020, **878**, 114602, DOI: [10.1016/j.jelechem.2020.114602](https://doi.org/10.1016/j.jelechem.2020.114602).
- 13 M. E. G. Lyons and G. P. Keeley, Immobilized Enzyme-Single-Wall Carbon Nanotube Composites for Amperometric Glucose Detection at a Very Low Applied Potential, *Chem. Commun.*, 2008, **22**, 2529–2531, DOI: [10.1039/b718863c](https://doi.org/10.1039/b718863c).
 - 14 M. M. Rahman, A. Umar and K. Sawada, Development of Amperometric Glucose Biosensor Based on Glucose Oxidase Co-Immobilized with Multi-Walled Carbon Nanotubes at Low Potential, *Sens. Actuators, B*, 2009, **137**(1), 327–333, DOI: [10.1016/j.snb.2008.10.060](https://doi.org/10.1016/j.snb.2008.10.060).
 - 15 K. Kojima and K. Sode, Review of Glucose Oxidases and Glucose Dehydrogenases: A Bird's Eye View of Glucose Sensing Enzymes, *J. Diabetes Sci. Technol.*, 2011, **5**(5), 1068–1076, DOI: [10.1177/193229681100500507](https://doi.org/10.1177/193229681100500507).
 - 16 S. D. Kumar, A. V. Kulkarni, R. G. Dhaneshwar and S. F. D'Souza, Cyclic Voltammetric Studies at the Glucose Oxidase Enzyme Electrode, *J. Electroanal. Chem.*, 1992, **342**(2), 153–160, DOI: [10.1016/0022-0728\(92\)85046-6](https://doi.org/10.1016/0022-0728(92)85046-6).
 - 17 S. Jin, I. Ryu, G. Choe, S. W. Song, H. M. Kim, D. Hong and S. Yim, Trade-off between Areal Capacitance and Optical Transmittance of Highly Transparent MnO₂ Electrodes for Supercapacitors, *J. Energy Storage*, 2022, **50**, 104641, DOI: [10.1016/j.est.2022.104641](https://doi.org/10.1016/j.est.2022.104641).
 - 18 T. Bi, H. Fang, J. Jiang, X. He, X. Zhen, H. Yang, Z. Wei and Z. Jia, Enhance Supercapacitive Performance of MnO₂/3D Carbon Nanotubes-Graphene as a Binder-Free Electrode, *J. Alloys Compd.*, 2019, **787**, 759–766, DOI: [10.1016/j.jallcom.2019.02.117](https://doi.org/10.1016/j.jallcom.2019.02.117).
 - 19 T. Lin, J. Lin, X. Wei, L. Lu and X. Yin, Hydrothermal Synthesis of Nano-Sized MnO₂ Supported on Attapulgite Electrode Materials for Supercapacitors, *Int. J. Hydrogen Energy*, 2022, **46**, 10765–10777, DOI: [10.1016/j.ijhydene.2022.12.151](https://doi.org/10.1016/j.ijhydene.2022.12.151).
 - 20 L. Hao, S.-S. Li, J. Wang, Y. Tan, L. Bai and A. Liu, MnO₂/Multi-Walled Carbon Nanotubes Based Nanocomposite with Enhanced Electrocatalytic Activity for Sensitive Amperometric Glucose Biosensing, *J. Electroanal. Chem.*, 2020, **878**, 114602, DOI: [10.1016/j.jelechem.2020.114602](https://doi.org/10.1016/j.jelechem.2020.114602).
 - 21 B. Usharani and V. Manivannan, Hydrothermal Synthesis of RGO-MnO₂ Nanocomposite: Characterization and in Vitro Biological Evaluation, *Mater. Lett.: X*, 2022, **15**, 100162, DOI: [10.1016/j.mlblux.2022.100162](https://doi.org/10.1016/j.mlblux.2022.100162).
 - 22 A. Hammami, I. Ben Assaker and R. Chtourou, Regenerative, low-cost and switchable photoelectrochemical sensor for detection of Cu²⁺ using MnO₂-GO heterojunction, *J. Solid State Electrochem.*, 2021, **26**, 211–218, DOI: [10.1007/s10008-021-05092-9](https://doi.org/10.1007/s10008-021-05092-9).
 - 23 P. Si, P. Chen and D.-H. Kim, Electrodeposition of Hierarchical MnO₂ Spheres for Enzyme Immobilization and Glucose Biosensing, *J. Mater. Chem. B*, 2013, **1**(21), 2696–2700, DOI: [10.1039/C3TB20341G](https://doi.org/10.1039/C3TB20341G).
 - 24 A. Kovalyk, O. Tananaiko, A. Borets, M. Etienne and A. Walcarius, Voltammetric and Microscopic Characteristics of MnO₂ and Silica-MnO₂ hybrid Films Electrodeposited on the Surface of Planar Electrodes, *Electrochim. Acta*, 2019, **306**, 680–687, DOI: [10.1016/j.electacta.2019.03.156](https://doi.org/10.1016/j.electacta.2019.03.156).
 - 25 V. V. Poltavets, V. F. Vargalyuk and L. Shevchenko, Express-Method for Estimation of Electrocatalytic Activity of Oxide Films toward Oxygen Transfer Reactions, *Univers. J. Chem. Publ.*, 2018, **6**(2), 15–20, DOI: [10.13189/ujc.2018.060201](https://doi.org/10.13189/ujc.2018.060201).
 - 26 V. V. Poltavets, V. F. Vargalyuk, V. A. Seredyuk and L. V. Shevchenko, The Mechanism of Electrooxidation of Mn⁺² Ions, *J. Chem. Technol.*, 2018, **26**(2), 1–11, DOI: [10.15421/0817260201](https://doi.org/10.15421/0817260201).
 - 27 H. Huang, W. Zhang, Y. Fu and X. Wang, Controlled Growth of Nanostructured MnO₂ on Carbon Nanotubes for High-Performance Electrochemical Capacitors, *Electrochim. Acta*, 2015, **152**, 480–488, DOI: [10.1016/j.electacta.2014.11.162](https://doi.org/10.1016/j.electacta.2014.11.162).
 - 28 A. Audi and P. Sherwood, Valence-Band X-Ray Photoelectron Spectroscopic Studies of Manganese and Its Oxides Interpreted by Cluster and Band Structure Calculations, *Surf. Interface Anal.*, 2002, **33**, 274–282, DOI: [10.1002/sia.1211](https://doi.org/10.1002/sia.1211).
 - 29 M. C. Biesinger, B. P. Payne, A. P. Grosvenor, L. W. M. Lau, A. R. Gerson, R. St and C. Smart, Resolving Surface Chemical States in XPS Analysis of First Row Transition Metals, Oxides and Hydroxides: Cr, Mn, Fe, Co and Ni, *Appl. Surf. Sci.*, 2011, **257**(7), 2717–2730, DOI: [10.1016/j.apsusc.2010.10.051](https://doi.org/10.1016/j.apsusc.2010.10.051).
 - 30 P. G. Perret, P. R. L. Malenfant, C. Bock and B. MacDougall, Electro-Deposition and Dissolution of MnO₂ on a Graphene Composite Electrode for Its Utilization in an Aqueous Based Hybrid Supercapacitor, *J. Electrochem. Soc.*, 2012, **159**(9), A1554, DOI: [10.1149/2.064208jes](https://doi.org/10.1149/2.064208jes).
 - 31 H. W. Nesbitt and D. Banerjee, Interpretation of XPS Mn (2p) spectra of Mn oxyhydroxides and constraints on the mechanism of MnO₂ precipitation, *J. Am. Mineral.*, 1998, **83**, 305–315, DOI: [10.2138/am-1998-3-414](https://doi.org/10.2138/am-1998-3-414).
 - 32 Q. Lv, S. Wang, H. Sun, J. Luo, J. Xiao, F. Xiao and S. Wang, Solid-State Thin-Film Supercapacitors with Ultrafast Charge/Discharge Based on N-Doped-Carbon-Tubes/Au-Nanoparticles-Doped-MnO₂ Nanocomposites, *Nano Lett.*, 2016, **16**(1), 40–47, DOI: [10.1021/acs.nanolett.5b02489](https://doi.org/10.1021/acs.nanolett.5b02489).
 - 33 J.-H. Jeong, J. W. Park, D. W. Lee, R. H. Baughman and S. J. Kim, Electrodeposition of α-MnO₂/γ-MnO₂ on Carbon Nanotube for Yarn Supercapacitor, *Sci. Rep.*, 2019, **9**, 11271, DOI: [10.1038/s41598-019-47744-x](https://doi.org/10.1038/s41598-019-47744-x).
 - 34 E. Turkusica, J. Kalcherb, E. Kahrovica, N. W. Beyenec, H. t. Modereggerc, E. Sofica, S. Begica and K. Kalcher, Amperometric determination of bonded glucose with an MnO₂ and glucose oxidase bulk-modified screen-printed electrode using flow-injection analysis, *Talanta*, 2005, **65**, 559–564, DOI: [10.1016/j.talanta.2004.07.023](https://doi.org/10.1016/j.talanta.2004.07.023).
 - 35 N. W. Beyene, P. Kotzian, K. Schachl, H. Alemu, E. Turkušić, A. Copra, H. Moderegger, I. Švancara, K. Vytras and K. Kalcher, (Bio)sensors based on manganese dioxide-modified carbon substrates: retrospections, further



- improvements and applications, *Talanta*, 2004, **64**, 1151–1159, DOI: [10.1016/j.talanta.2004.03.068](https://doi.org/10.1016/j.talanta.2004.03.068).
- 36 B. Zhu, W. Li, N. Chi, R. V. Lewis, J. Osamor and R. Wang, Optimization of Glutaraldehyde Vapor Treatment for Electrospun Collagen/Silk Tissue Engineering Scaffolds, *ACS Omega*, 2017, **2**(6), 2439–2450, DOI: [10.1021/acsomega.7b00290](https://doi.org/10.1021/acsomega.7b00290).
- 37 O. Barbosa, C. Ortiz, Á. Berenguer-Murcia, R. Torres, R. C. Rodrigues and R. Fernandez-Lafuente, Glutaraldehyde in Bio-Catalysts Design: A Useful Crosslinker and a Versatile Tool in Enzyme Immobilization, *RSC Adv.*, 2013, **4**(4), 1583–1600, DOI: [10.1039/C3RA45991H](https://doi.org/10.1039/C3RA45991H).
- 38 E.-K. Yan, H.-L. Cao, C.-Y. Zhang, Q.-Q. Lu, Y.-J. Ye, J. He, L.-J. Huang and D.-C. Yin, Cross-Linked Protein Crystals by Glutaraldehyde and Their Applications, *RSC Adv.*, 2015, **5**(33), 26163–26174, DOI: [10.1039/C5RA01722J](https://doi.org/10.1039/C5RA01722J).
- 39 J. G. Ayenimo and S. B. Adeloju, Amperometric Detection of Glucose in Fruit Juices with Polypyrrole-Based Biosensor with an Integrated Permselective Layer for Exclusion of Interferences, *Food Chem.*, 2017, **229**, 127–135, DOI: [10.1016/j.foodchem.2017.01.138](https://doi.org/10.1016/j.foodchem.2017.01.138).
- 40 C. He, M. Xie, F. Hong, X. Chai, H. Mi, X. Zhou, L. Fan, Q. Zhang, T. Ngai and J. Liu, A Highly Sensitive Glucose Biosensor Based on Gold Nanoparticles/Bovine Serum Albumin/Fe₃O₄ Biocomposite Nanoparticles, *Electrochim. Acta*, 2016, **222**, 1709–1715, DOI: [10.1016/j.electacta.2016.11.162](https://doi.org/10.1016/j.electacta.2016.11.162).
- 41 L. Zhang, S. Yuan, L. Yang, Z. Fang and G.-C. Zhao, An Enzymatic Glucose Biosensor Based on a Glassy Carbon Electrode Modified with Manganese Dioxide Nanowires, *Microchim. Acta*, 2013, **180**, 627–633, DOI: [10.1007/s00604-013-0968-9](https://doi.org/10.1007/s00604-013-0968-9).
- 42 V. Vukojević, S. Djurdjić, M. Ognjanović, M. Fabián, A. Samphao, K. Kalcher and D. M. Stanković, Enzymatic Glucose Biosensor Based on Manganese Dioxide Nanoparticles Decorated on Graphene Nanoribbons, *J. Electroanal. Chem.*, 2018, **823**, 610–616, DOI: [10.1016/j.jelechem.2018.07.013](https://doi.org/10.1016/j.jelechem.2018.07.013).
- 43 V. N. Nikitina, A. R. Karastsialiova and A. A. Karyakin, Glucose test strips with the largest linear range made via single step modification by glucose oxidase-hexacyanoferrate-chitosan mixture, *Biosens. Bioelectron.*, 2023, **220**, 114851, DOI: [10.1016/j.bios.2022.114851](https://doi.org/10.1016/j.bios.2022.114851).

